Crashworthiness improvements of multi-cell thin-walled tubes through lattice structure enhancements

Hu Liu[1], Zheng Xian Caleb Chng[1], Guangjian Wang[1,2], Bing Feng Ng[1*]

[1]*School of Mechanical and Aerospace Engineering, Nanyang Technological University, 50 Nanyang Avenue, Singapore 639798, Singapore*

[2]*Singapore Centre for 3D Printing, School of Mechanical and Aerospace Engineering, Nanyang Technological University, 50 Nanyang Avenue, Singapore, 639798, Singapore*

Abstract

Taking advantage of multi-cell tubes and lattice structures on improving crashworthiness performances, a novel multi-cell thin-walled tube filled with uniform and graded lattice structures is explored in this paper. The body-centered cubic lattice structure is employed as the uniform lattice filler, while the graded lattice filler is constructed by varying the diameter of lattice rods in each layer. Several geometric parameters are investigated numerically, which include the cell number of tube, the dimension of tube and lattice, the height-to-width ratio of the enhanced tube, and the configuration of graded lattices. These parameters are then compared for their crushing load-displacement curves, deformation modes, and energy-absorbing mechanisms. It is observed that the multi-cell tubes exhibit significant improvements to the absorbed energy and crushing force efficiency over the single-cell tubes. In addition, the specific energy absorption (SEA) of the hybrid multi-cell tube structures is improved by 78.6% with respect to the sum of its individual constituents. Furthermore, the multi-cell tube structure filled with graded lattices can present larger energy-absorbing capacity than its uniform lattice counterpart, and the strong end at its top provides better SEA performance. Overall, the hybrid lattice-enhanced tube structure provides an optimal strategy for the crashworthiness design of multi-cell tubes, which can serve as a potential candidate for future crashworthiness applications.

Keywords: dynamic response; multi-cell tube; thin-walled structure; lattice structure; crashworthiness; energy absorption.

* Corresponding author.

E-mail address: bingfeng@ntu.edu.sg (Bing Feng Ng).

1. Introduction

The global interest in transport engineering has been oriented towards designing lightweight components with efficient crashworthiness characteristics without compromising on occupant safety. Particularly, thin-walled tubes are widely employed as energy absorption devices due to their high energy absorption capabilities and stable deformation modes under crushing loads. Recently, extensive attention has been paid to study the energy absorption capabilities of thin-walled tubes with different cross-sectional configurations, such as square [1-4], circular [5-8], octagonal [9], triangular [10] and other irregular cross-sectional shapes [11-13]. These studies demonstrate that the circular cross-sectional tube can provide better energy absorption capability as compared to other cross-sectional configurations [14]. Besides, to further enhance the energy absorption capability of single-cell tube structures, the tapered [15, 16], conical [17] and folded [18, 19] tubes were also proposed and investigated by several researchers through analytical, numerical and experimental means.

Apart from varying the cross-sectional configurations of traditional single-cell tube structures, multi-cell designs are also conceptualized to enhance the crashworthiness performance of thin-walled structures. For instance, Kim [20] proposed multi-cell tube structures that presented dramatic improvements to crash energy absorption and weight efficiency against the conventional square single tubes. Similar studies were also systematically carried out by Zhang et al. [21-23], who concluded that multi-cell structures can greatly enhance axial crush resistance and energy absorption characteristics. Moreover, other multi-cell thin-walled tubes inspired by micro-configuration of biological tissue were shown to improve crashworthiness capacities [24-29]. Apart from the axial compressive load [30-32], the dynamic responses of multi-cell tube structures subject to oblique [33], lateral [34], and bending loadings [35-37] were also widely investigated. All these studies demonstrated that multi-cell tubes can outperform single-cell tubes in terms of crashworthiness.

To further enhance the crushing resistance and deformation stability of thin-walled structures, the internal empty spaces can be filled with lightweight components such as metallic foam. For instance, Santosa et al. [38] studied the crushing behavior of aluminum foam-filled square columns, in which the formula for the mean crushing force was proposed and good agreement was achieved between experimental and numerical predictions. Similarly, Duarte et al. [39] analyzed

the dynamic response of square polymer-aluminum alloy hybrid foam-filled thin-walled tubes, and significantly higher energy absorption density and specific energy absorption capacity was achieved as compared to empty tubes. The conclusions were also validated by several other experimental, numerical, and analytical investigations [40-46]. Besides, honeycomb [47, 48] and concrete [49-51] materials were also employed as fillers to enhance the mechanical behaviors of thin-walled tubes. These studies indicate that foam and honeycomb are two effective lightweight materials to enhance the crashworthiness of thin-walled tubes.

With developments in additive manufacturing techniques that allow for more complicated geometrical features [52-54], the lattice structure becomes another ideal filler material to improve the crashworthiness of thin-walled tubes. In the pioneering works of Cetin and Baykasoğlu [55, 56], the mechanical behaviors of thin-walled tubes were enhanced by inserting lattice structures, and 115% higher impact energy was achieved for the hybrid structures as compared to the sum of its individual parts. Meanwhile, graded lattice structures were also adopted to enhance the crashworthiness performances of thin-walled tubes [57, 58]. As a novel filler material, most works only considered lattice structures as fillers in single tubes, and their potential application on multi-cell tubes still needs to be explored.

In fact, substantial efforts have been devoted to investigating the multi-cell tube structures filled by foam and other cellular materials. For instance, Chen and Wierzbicki [59] analytically and numerically studied the axial crushing behaviors of multi-cell thin-walled tubes filled with foam materials and found that the interaction between the foam core and the tube wall contributed greatly to the total crushing resistance of multi-cell tubes. Googarchin et al. [60] examined the enhanced energy absorption performance of tapered multi-cell tubes filled with foam materials, while the improved crushing behavior of multi-cell tubes filled with honeycomb was investigated by Zhang et al. [61]. Meanwhile, improvements in the crashworthiness of multi-cell tubes with lightweight material fillings were also reported by several other authors [62-65]. However, no available studies have been conducted thus far on the dynamic crushing response of multi-cell tubes filled with lattice materials.

In this work, the uniform and graded Lattice-Enhanced Multi-cell Tubes (LEMTs) are proposed to further explore the crashworthiness of tube-type structures. The numerical model is first validated by comparing with previous experiments to determine the ability of the present

numerical approach in predicting the interaction between lattice filler and tube. Subsequently, in-depth analysis is performed on the effects of design parameters on crashworthiness performances of the hybrid LEMT structures, with parameters that include the cell number of tube, the dimension of tube and lattice, the height-to-width ratio of the enhanced tube, and the configuration of graded lattices. This study presents fundamental understandings in the design and crushing mechanism of lattice structures in multi-cell tubes for application in transport engineering and other dynamic environments.

2. Multi-cell thin-walled tube filled with lattice structure

The hybrid LEMT structure is constructed by filling the hollow cross-sections of multi-cell thin-walled tubes with lattice structures. Both uniform lattice and graded lattice with varying rod diameters across different layers are taken into account. The multi-cell thin-walled tubes are comprised of 1×1, 2×2 and 3×3 cells. Detailed geometrical descriptions of the multi-cell thin-walled tube and lattice structures are discussed in the following sub-sections.

2.1. Configuration of multi-cell thin-walled tube

The thin-walled tube structures adopted in this study are presented in Fig. 1, in which the 3×3 and 2×2 structures are multi-cell tubes and 1×1 structure represents the single-cell tube. The height of the multi-cell tubes is kept constant while the length L and width W are variables depending on the number of tube cells. This is to ensure that the number of filled lattice unit along the height of the tube can be kept constant as the cell number of tubes is increased. As shown in Fig. 1, each cell of tube has a square cross-section with length L_u and width W_u, both equaling to 20 mm. Accordingly, the total dimensions for the 3×3, 2×2 and 1×1 thin-walled tubes are 60 mm × 60 mm, 40 mm × 40 mm and 20 mm × 20 mm, respectively. The height H and thickness t of the multi-cell thin-walled tubes are set as 120 mm and 0.5 mm, respectively, unless otherwise specified.

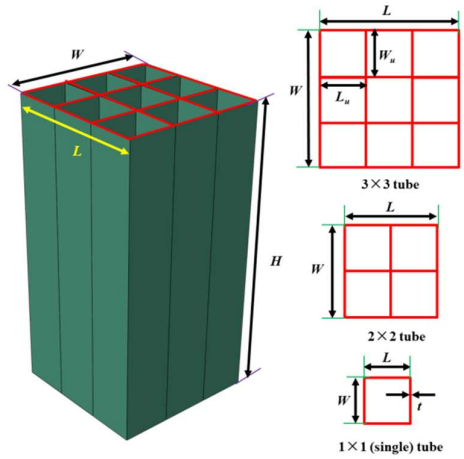

Fig. 1. Schematics of multi-cell thin-walled tube with different cell numbers.

2.2. Configuration of lattice structure

In this study, the body-centered cubic (BCC) lattice structure is chosen to fill the multi-cell thin-walled tubes. To ensure that the lattice structure fits exactly inside the hollow cross-section of each thin-walled tube, the width of the BCC lattice structure b is designed to be slightly smaller than the internal width of the thin-walled tube, i.e., $b \leq W_u - t$ in Fig. 1. In addition, the total height of the BCC lattice structure is equal to that of the multi-cell tube.

Both uniform and graded BCC lattice structures are taken into account, which comprise of six layers of BCC unit with an equivalent height of $H_u = H/6$ and width b = 19.5 mm, as shown in Fig. 2. For the uniform BCC lattice, the diameter of lattice rod d for each layer is the same. For the graded lattice structure, it is constructed by varying the lattice rod diameter for each layer, in which the lattice rod diameter at the bottom can be calculated as a function of that at the top. This can be expressed as [58]

$$d_{bottom} = d_{top} - 2\sqrt{3}b\tan\alpha \tag{1}$$

in which d_{top} and d_{bottom} represent the diameter of the lattice rod in the top and bottom layers, respectively; b is the width of the BCC lattice unit, and α represents the taper angle. The configurations of the graded lattice structure with different taper angles are presented in Fig. 2, which demonstrates that the lattice rod diameter of the bottom layer d_{bottom} decreases as the value of taper angle α is increased.

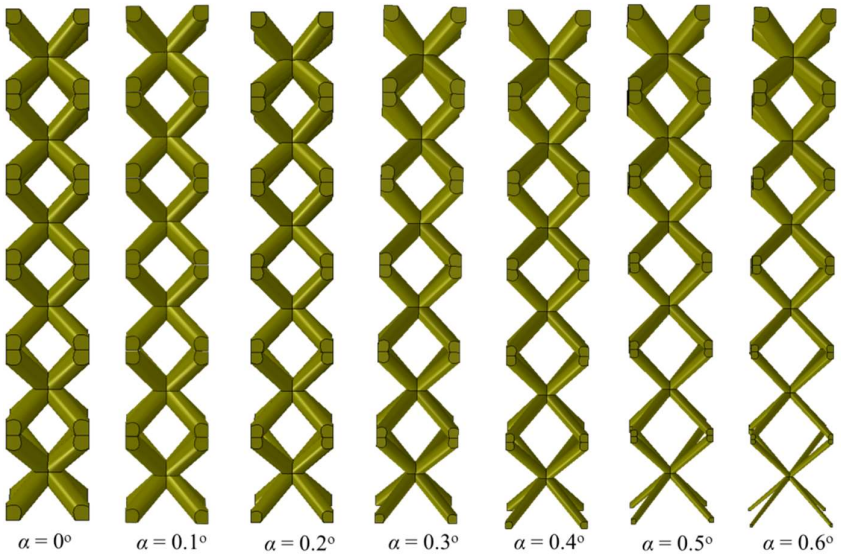

Fig. 2. Lattice structure with different taper angles. The lattice rod diameter of the bottom layer decreases as the taper angle is increased.

2.3. Hybrid LEMT structures

The hybrid LEMT structure is formed by filling the hollow cross-section of each multi-cell tube with lattice structures, as shown in Fig. 3. In practice, the multi-cell tube and lattice structures can be manufactured separately with additive manufacturing as an option for the latter. The hybrid LEMT structure is then established by combining the two parts together, as presented in Fig. 3. It is assumed that the lattice structures are perfectly straight and its BCC units have constant width and height. To avoid the potential fracture of the tube wall caused by the filling lattice rod during the crushing process, the edge of each rod is trimmed into a plane to ensure it is parallel to the internal wall of the multi-cell tube, as shown in Fig. 3.

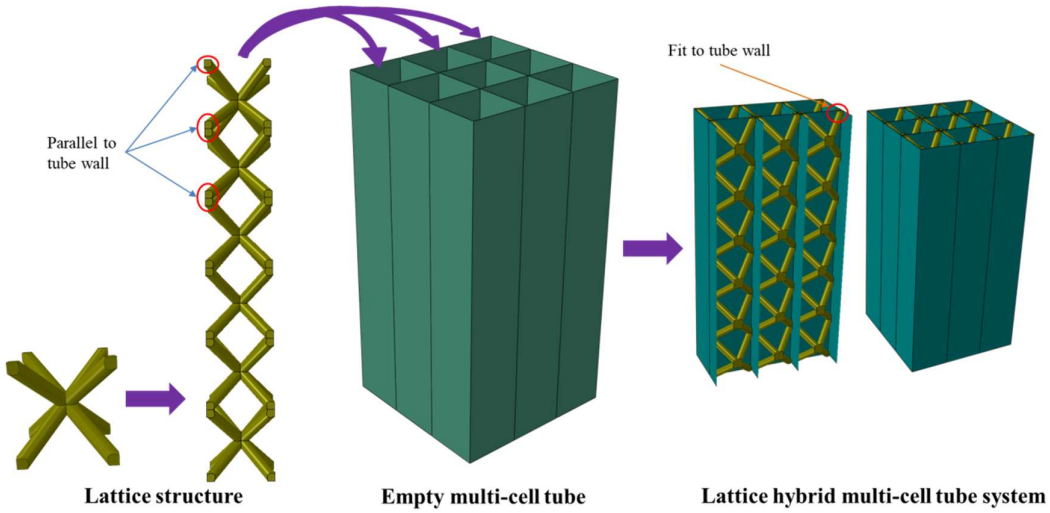

Fig. 3. Schematics for the hybrid LEMT structure with illustration on the assembly of lattice structures into the empty multi-cell tubes.

3. Methodology

Finite element (FE) simulations are carried out to assess the crashworthiness performance of hybrid LEMT structures. Different performance indicators such as peak crushing force, specific energy absorption, maximum crushing displacement and crushing force efficiency are used to reflect and compare hybrid LEMT structures of different geometrical parameters. The numerical modeling for the crushing simulation and the crashworthiness performance indicators will be discussed in detail in this section.

3.1. Numerical modeling

The FE simulations are performed using the commercial software ABAQUS/Explicit package. The multi-cell thin-walled tube is built using 4-node linear shell element with reduced-integration (S4R), while the 4-node linear tetrahedral element with reduced integration (C3D4R) is employed for the lattice structures. As shown in Fig. 4, the hybrid LEMT structure is sandwiched between two rigid plates, in which the bottom is fixed without movement, and the top is moving downwards with a constant velocity of 10 m/s. The initial geometric imperfection of the multi-cell tube is taken into account by using the eigenvalue buckling simulation [55], in which its buckling mode magnitude is set as 0.02 of the tube thickness. The interaction between the lattice structure and thin-walled tube, as well as the interactions between the hybrid LEMT structures and the rigid plates are all defined as general contact property to ensure the LEMT structures do not penetrate the top and bottom rigid plates and the inner lattice not penetrate the tube walls during the

crushing process. The friction coefficient can reflect the contact behaviors among different contact pairs. Here, all contacts are defined by using the penalty formulation with friction coefficient of 0.25 [55] in the tangential direction and 'hard contact' in the normal direction.

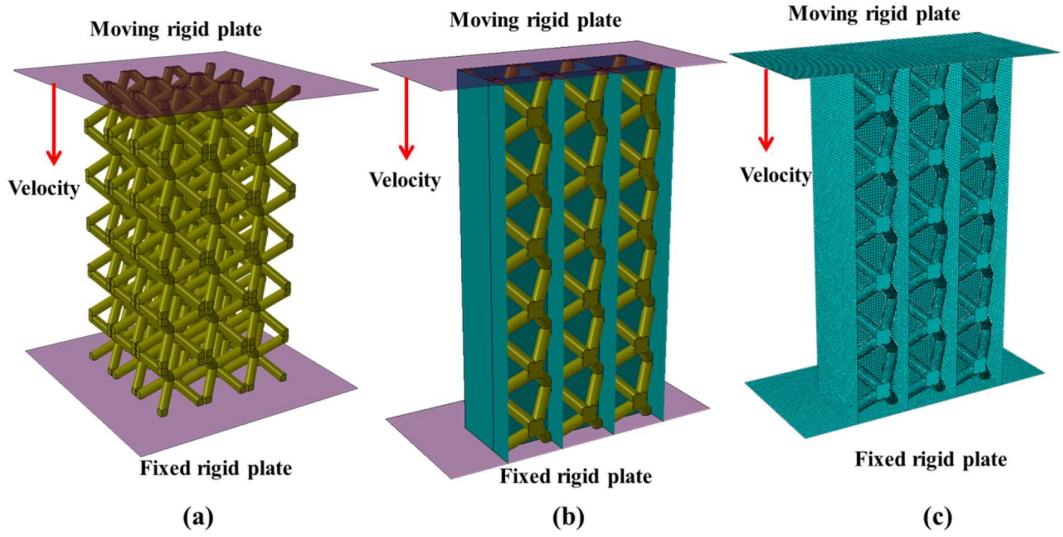

Fig. 4. Analysis model for (a) lattice only and (b) hybrid LEMT structure as well as (c) its finite element model.

A mesh sensitivity study is first conducted to ensure that reasonable element sizes for the thin-walled tubes and lattices are used for subsequent simulations. Considering a hybrid single tube, Fig. 5(a) compares the force-displacement curves for different element sizes on the lattice structure while keeping the size of elements on the thin-walled tube constant. Separately, Fig. 5(b) compares the force-displacement curves for different element sizes on the thin-walled tube while keeping the element size of lattice constant. Four different element sizes for the lattice, i.e., 0.3 mm, 0.6 mm, 0.9 mm, and 1.2 mm, and four different element sizes for the thin-walled tube, i.e., 1 mm, 2 mm, 3 mm, and 4 mm are employed for the convergence study. It is found that deviations in the force-displacement curves are small for the different element sizes considered here. For computational accuracy, the average element sizes for the thin-walled tube and lattice structure are set as 1 mm and 0.3 mm, respectively. As a result, the FE model of the 3×3 hybrid LEMT structure has a total of 418,104 elements, as depicted in Fig. 4(c).

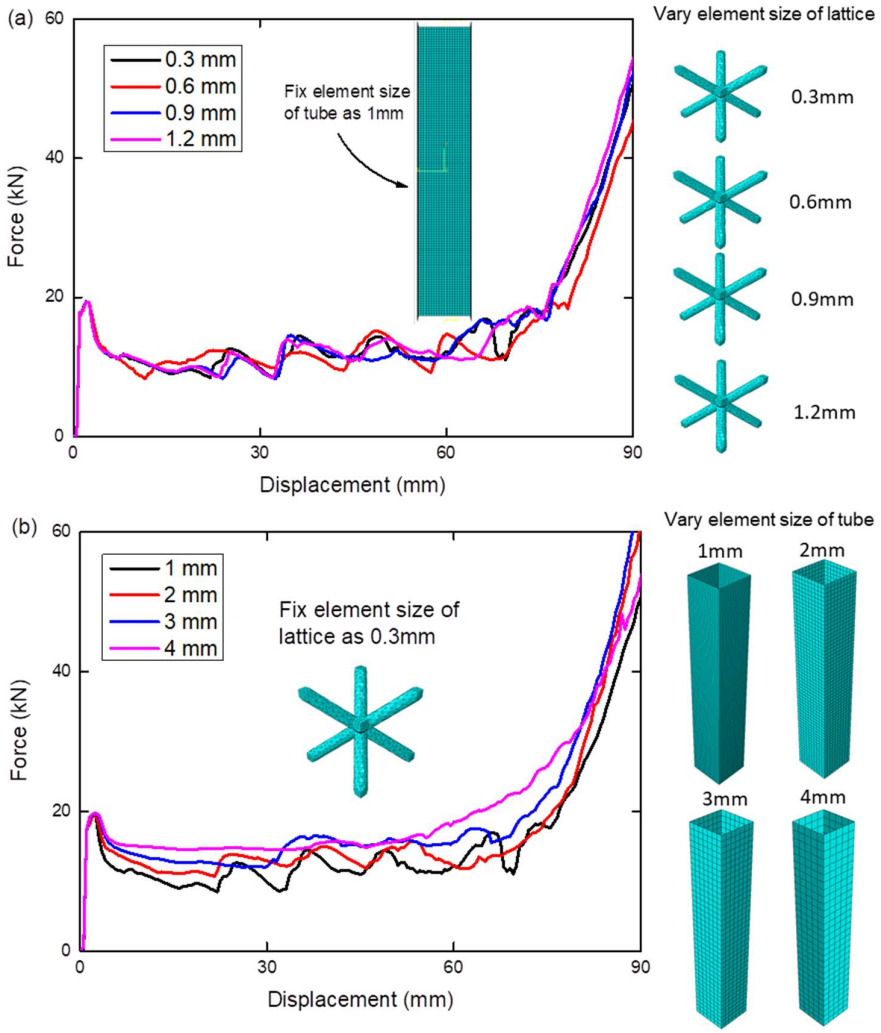

Fig. 5. Force-displacement curve of hybrid tube structure with varying element size of (a) lattice and (b) thin-walled tube.

The materials for the thin-walled tube and lattice structure are both defined as aluminum alloy Al6063-T5, which has mass density ρ = 2700 kg/m^3, Young's modulus E = 68.2 GPa, yield strength σ_y = 187 MPa, and Poisson's ratio v = 0.3. Besides, the Cowper Symonds power-law constitutive model is used to define the hardening behavior of the material, which can be expressed as [55]

$$\frac{\sigma_{dyn}}{\sigma_{stat}} = R = 1 + \left(\frac{\dot{\varepsilon}}{D}\right)^{1/n} \tag{2}$$

in which σ_{dyn} and σ_{stat} are, respectively, the dynamic and quasi-static strengths of the material, and R is the ratio of dynamic stress to the static flow stress. $\dot{\varepsilon}$ denotes the von-Mises equivalent plastic strain rate, while D and n are material constants. Clearly, the strain-rate sensitivity of the

material due to plasticity can be considered by using this equation. Herein, D = 128,800 s^{-1} and n = 4 are employed for the material of Al6063-T5 [66].

3.2. Crashworthiness performance indicators

To quantify the crashworthiness performance of hybrid LEMT structures under axial compression, several crashworthiness indicators are employed. The peak crushing force (PCF) can be obtained directly from the force-displacement curve, while the total energy absorption (EA) of the hybrid LEMT structure can be expressed as

$$EA = \int_0^{\xi_{\max}} F(\xi)\mathrm{d}\xi \tag{3}$$

where ξ is the crushing distance of the hybrid LEMT structure. ξ_{max} stands for the maximum crushing distance that can be obtained when the hybrid LEMT structure just reaches the densification region.

The specific energy absorption (SEA) represents energy absorbed per unit mass, calculated as

$$SEA = EA / m_{total} \tag{4}$$

in which m_{total} denotes the total mass of the hybrid LEMT structures. In fact, SEA can be treated as the criterion to represent the weight efficiency of structural crashworthiness.

The average crushing force (ACF) is defined as the ratio of EA to the maximum crushing distance $\xi_{\max}$, i.e.,

$$ACF = EA / \xi_{\max} \tag{5}$$

The crushing force efficiency (CFE) can be formulated as

$$CFE = ACF / PCF \tag{6}$$

which is an important indicator for evaluating the uniformity of the crush loads.

4. Validation studies

In this section, validation studies are performed on two cases to determine the effectiveness of the numerical method on predicting the dynamic crushing behaviors of hybrid LEMT structures. The first validation case examines the applicability of this method to analyze the interaction behaviors between lattice and tube structures, and the second validation case checks the validity of the numerical model in predicting the dynamic behavior of multi-cell thin-walled tubes.

4.1. Crushing response of lattice-enhanced single tube

The lattice-enhanced single tube under crush loading is investigated to determine whether the

interactions between the filled lattice and tube can be captured by comparing to Cetin and Baykasoğlu's experimental work [55]. Here, the hybrid structure is made of Al6063-T5 square tube and AlSi10Mg lattice with their materials given in Ref. [55]. The single tube structure with a 20 × 20 mm external dimension and a thickness value of 1.5 mm is taken into account. The size of the BCC lattice unit is $L_u = W_u = H_u = 16.5$ mm and a total of four BCC units are adopted. Similar to their experiment, the quasi-static loading condition with a crushing velocity of 2 mm/min is adopted in the simulations. As illustrated in Fig. 6, the final deformation modes of the hybrid single tube predicted by FE simulations are consistent with the experimental results. In addition, the elastic, elastic-plastic, plateau, densification phases in the force-displacement curve predicted by the FE simulation agree well with those obtained by experiment, which demonstrates that the present FE model can capture the interaction effects between the lattice and tube structures during the crushing.

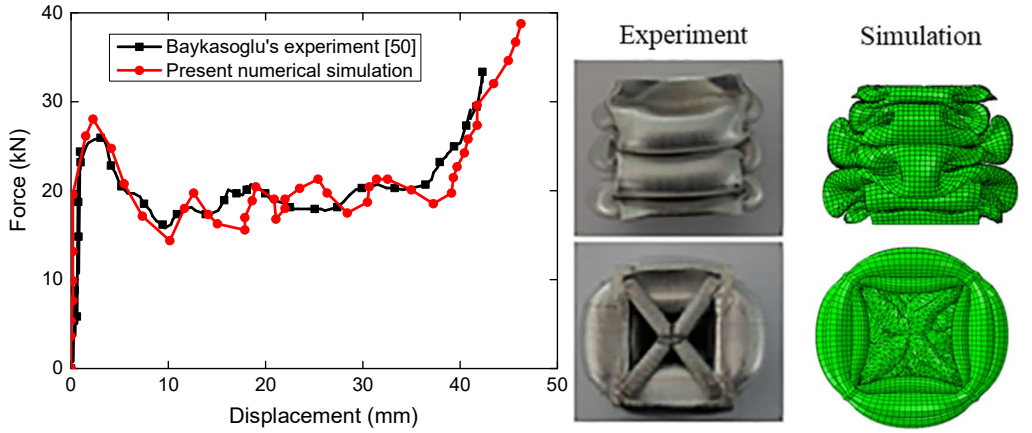

Fig. 6. Comparison between experiment [55] and present numerical simulation for force-displacement curve (left) and deformation mode (right) of lattice-enhanced single tube under crushing.

4.2. Crushing response of empty multi-cell tube

Here, the dynamic response of empty multi-cell thin-walled tube subjected to a crushing load is analyzed and compared to the experiment results by Zhang and Zhang [67]. In their experiments, the bottom of the tube is welded to a supported end, and the top end is acted on by a compressive load. Similar condition with a fixed bottom is employed in the FE modeling process. The dimensions of the single and 2×2 multi-cell tubes are $L = W = 36$ mm and $H = 115$ mm, and the thickness of the tubes is $t = 1.2$ mm. Similar to Ref. [67], the tube is made of AA6061-O with Young's modulus $E = 68$GPa and Poisson's ratio $v = 0.33$. Power-law hardening behavior with exponent $n = 0.18$, initial yield stress $\sigma_y = 71$ MPa and ultimate stress $\sigma_u = 131$ MPa are employed.

The crushing force and deformation modes of single and multi-cell empty tubes predicted by the simulations are compared to the experiments in Fig. 7. One can find that the FE model can capture the initial peak force both for the single-cell and 2×2 multi-cell tubes. As shown in Fig. 7(a), slight deviations are observed in the second and following folds for the single-cell tube. This may be caused by the following two reasons: firstly, the boundary condition in FE simulation (fixing the bottom end of the single tube) is slightly different from the welded end in the experiment. Secondly, the material imperfection from the experiments that is not captured by the FE simulation. However, for the 2×2 multi-cell tube in Fig. 7(b), this deviation is small, illustrating that the present numerical method possesses sufficient accuracy to investigate the crushing mechanism of multi-cell thin-walled tubes.

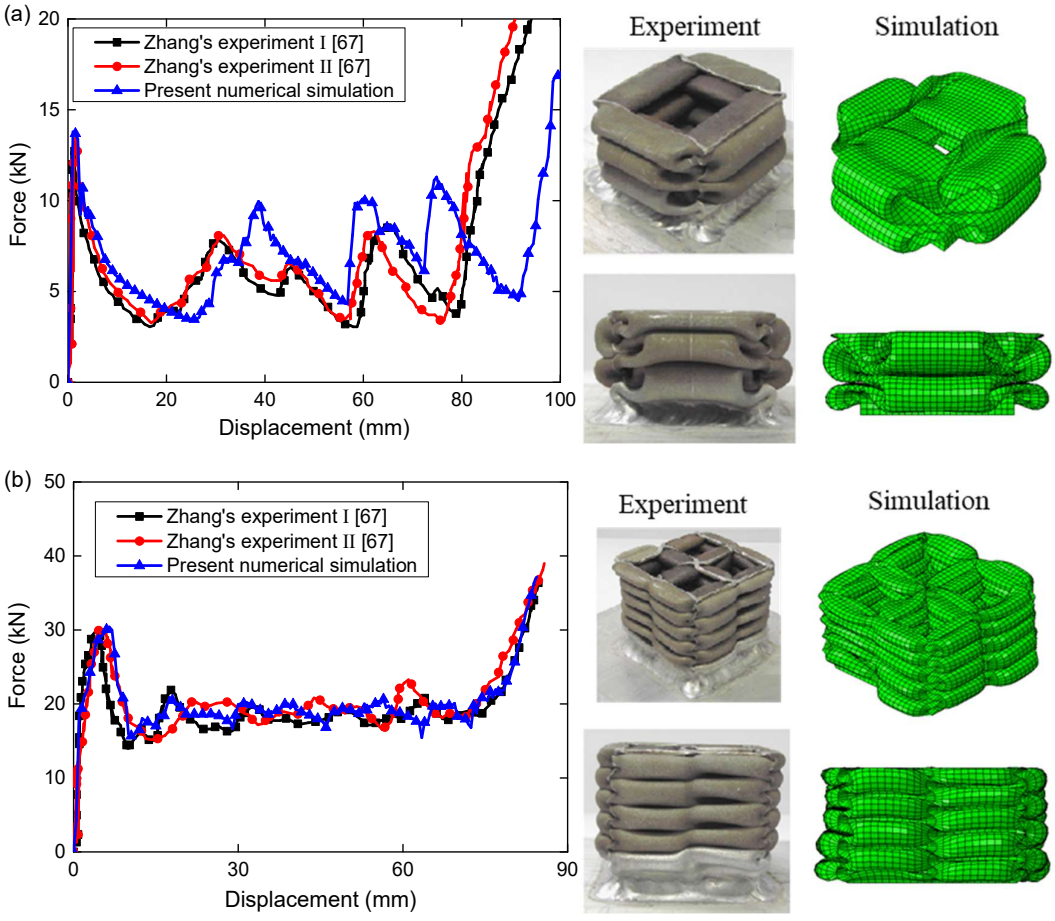

Fig. 7. Comparison between experiment [67] and present numerical simulation for force-displacement curve (left) and deformation mode (right) of empty multi-cell tube under crushing: (a) single tube; (b) 2×2 multi-cell tube.

5. Results and discussion

In this study, several parameters including the number of cells in the tube, the dimensions of tube and lattice, the height-to-width ratio of the enhanced tube, the uniform and graded lattice structures, and the configuration of graded lattice (taper angle α) on the crashworthiness performance of hybrid LEMT structures will be examined. A summary of the case studies is presented in Fig. 8.

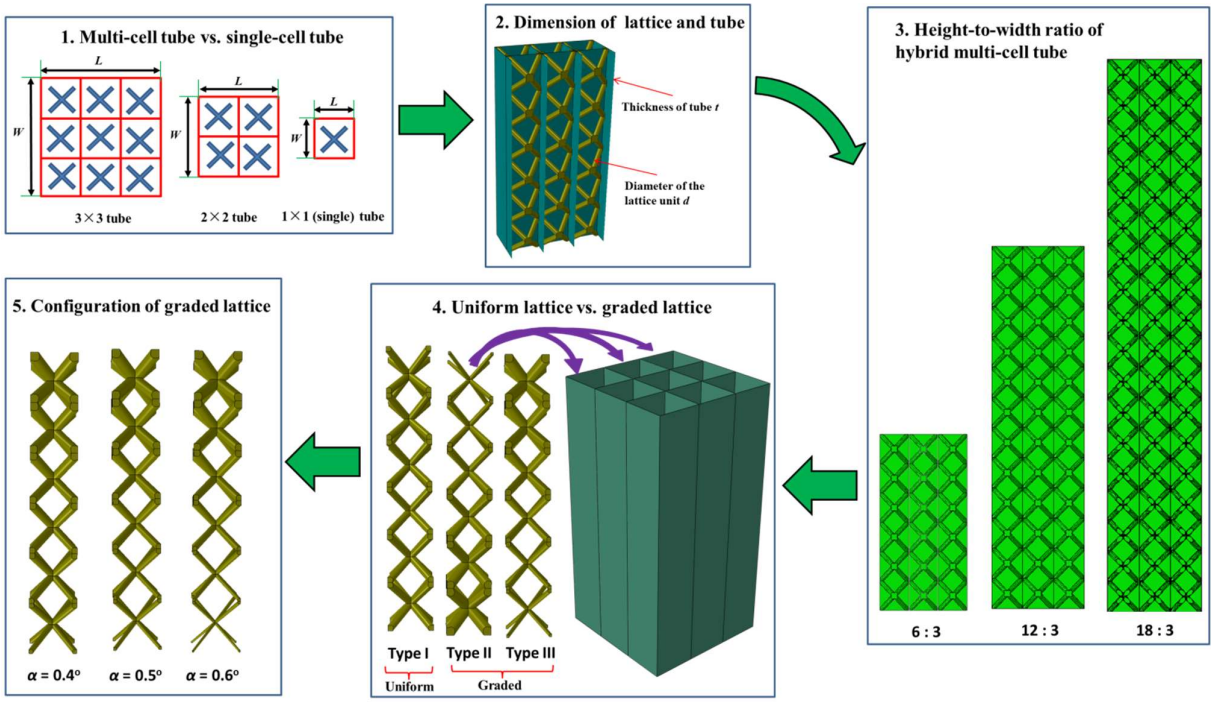

Fig. 8. Case studies for the hybrid LEMT structure, including the number of cells in the tube, the dimensions of tube and lattice, the height-to-width ratio of the enhanced tube, the uniform and graded lattice structures, and the configuration of graded lattice.

When the lattice and tube are assembled in the hybrid LEMT structure, it exhibits combined properties that result from mutual interactions. For comparisons, the direct summation of its constituents (i.e., the empty tube and the lattice) for the crushing force (F), EA, SEA, and CFE are further introduced and defined as follows

$$F_{tube+lattice} = F_{tube} + F_{lattice} \tag{7}$$

$$EA_{tube+lattice} = EA_{tube} + EA_{lattice} \tag{8}$$

$$SEA_{tube+lattice} = \frac{EA_{tube} + EA_{lattice}}{m_{tube} + m_{lattice}} \tag{9}$$

$$CFE_{tube+lattice} = \frac{ACF_{tube} + ACF_{lattice}}{PCF_{tube} + PCF_{lattice}} \tag{10}$$

in which the subscripts ‘tube’ and ‘lattice’ represent the empty tube and lattice structures,

respectively. For example, m_{tube} and $m_{lattice}$ are the mass of empty tube and lattice structures, respectively.

5.1. Single vs. multi-cell tube

The crushing force and energy absorption against the crushing displacement curves for the empty tube, lattice-only, sum of empty tube and lattice, and hybrid LEMT structures are plotted in Fig. 9 for different cell numbers. Here, the wall thickness t = 1 mm and lattice rod diameter d = 3 mm are employed. As observed, the lattice-only structures exhibit relatively small force-displacement characteristics with a long plateau and no obvious peaks due to the lack of any vertical members. This leads to a generally smooth and continuous crushing behavior that is very similar to the crushing behavior of foam structures [68]. Accordingly, the force-displacement curves for the sum of empty tubes and lattice structures exhibit similar trends as the empty tube.

However, the energy absorption of hybrid LEMT structures is significantly enhanced as compared to the summation of their individual components due to the interaction between the tube and lattice structures, while the PCF is almost unchanged. This indicates that filling lattice structures in the multi-cell tube is an effective approach for crashworthiness design. Even though the maximum crushing distance ξ_{max} at which the hybrid LEMT structure reaches the densification region is reduced as the cell number increases, the absorbed energy is still greatly enhanced as the number of cells is increased. Moreover, the enhancement of energy absorption δEA with respect to the sum of tube and lattice is increased by increasing the cell number of hybrid LEMT structures.

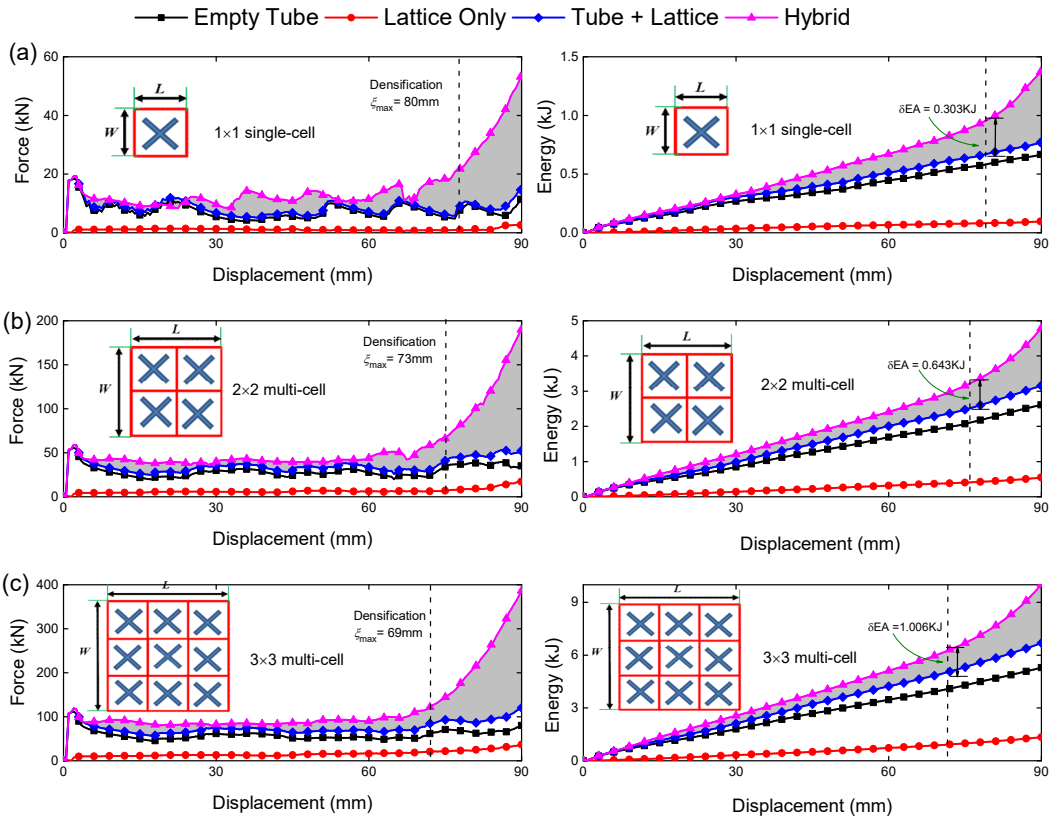

Fig. 9. Force-displacement and EA-displacement curves for hybrid LEMT structures with different cell numbers: (a) 1×1 single-cell; (b) 2×2 multi-cell; (c) 3×3 multi-cell. The grey shaded area denotes the enhanced force and EA of hybrid LEMT structures with respect to the summation of their individual constituents. As the cell number increases, the maximum crushing distance ξ_{max} is reduced, while the enhancement of energy absorption δEA is increased.

The SEA and CFE of hybrid LEMT structures with different cell numbers are depicted in Fig. 10, in which the empty tube, sum of empty tube and lattice, as well as the hybrid structures are compared. It is found that the hybrid LEMT structures provide significantly larger SEA and CFE as compared to empty tube structures. The SEA and CFE of hybrid LEMT structures are both enhanced as the cell number is increased. The SEA of the 3×3 hybrid LEMT structure is up to 78.6% higher than the sum of its individual components. The enhancements in CFE of hybrid LEMT structures with respect to the sum of their individual components are up to 27.3% and 25.9% for the 2×2 and 3×3 configurations, respectively. This suggests that cell number can enhance SEA and CFE significantly due to the interaction between the tube and lattice structures, which is helpful for the crashworthiness design of tube structures.

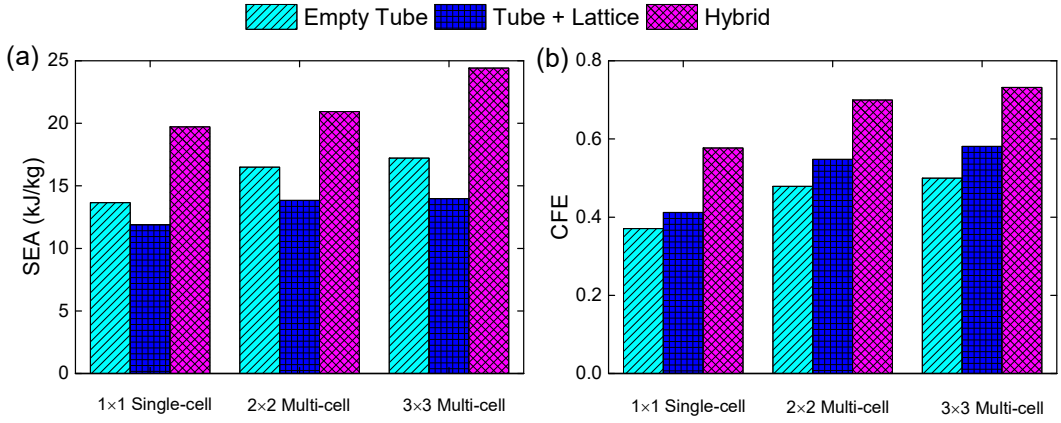

Fig. 10. (a) SEA and (b) CFE of hybrid LEMT structure with different cell numbers. As illustrated, the SEA and CFE are both enhanced as the cell number increases. The SEA and CFE of 3×3 hybrid LEMT structure are, respectively, 78.6% and 25.9% higher than the sum of its individual components.

In addition, the deformation processes for the hybrid LEMT structure with different cell numbers undergoing dynamic crushing are presented in Table 1. Clearly, the deformation first appears in the middle of the structure for all cell numbers, followed with layer by layer deformation during the crushing, i.e., progressive deformation pattern can be observed. More folding knots can be observed in the hybrid multi-cell tube as compared to the single tube due to the interaction between the center tube wall and inside lattice fillers.

Table 1. Deformation process of hybrid LEMT structure with different cell numbers. More folding knots can be observed in the hybrid multi-cell tube as compared to the single tube due to the interaction between the center tube wall and inside lattice fillers.

Type	$\varepsilon = 0$	$\varepsilon = 0.3$	$\varepsilon = 0.5$	$\varepsilon = 0.7$
1×1 single-cell	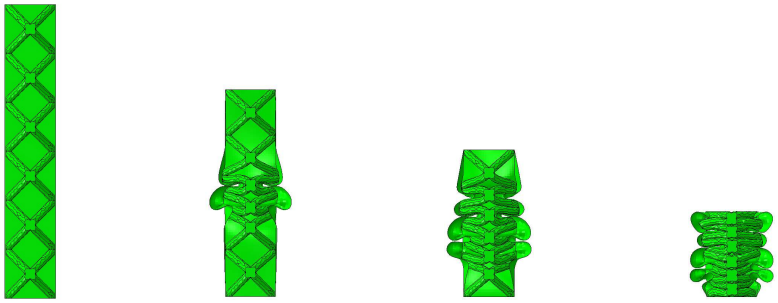			

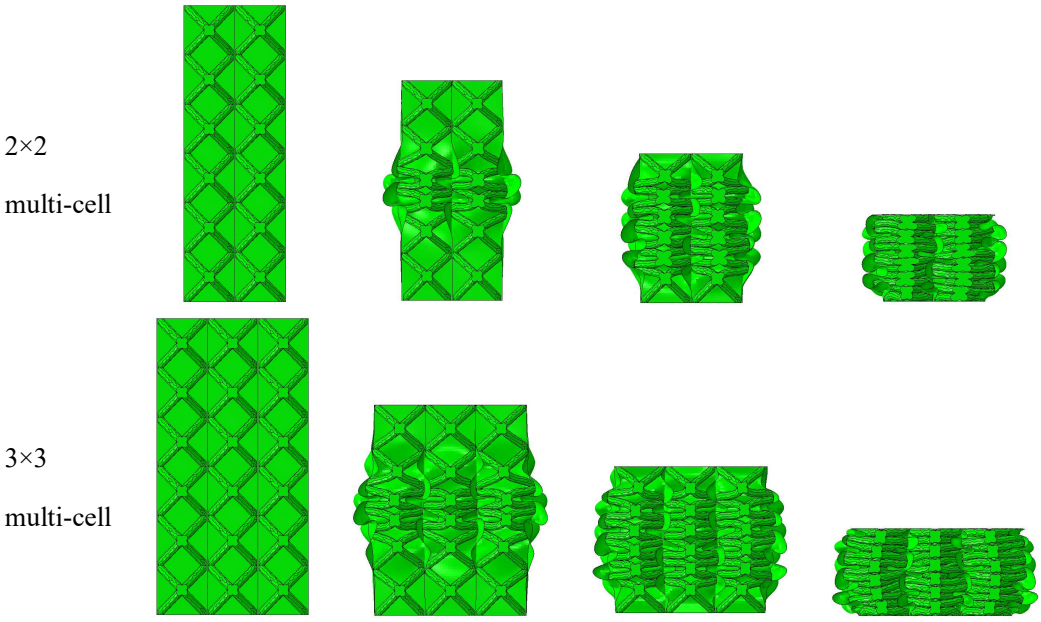

5.2. Dimension of lattice and multi-cell tube

The influence of geometrical parameters including tube wall thickness t and the lattice rod diameter d on the hybrid LEMT structure with 3×3 multi-cell configuration is investigated. Fig. 11 shows the force-displacement and EA-displacement curves for different lattice rod diameters under a constant wall thickness of t = 0.5 mm. As observed, both the crushing force and energy absorption are increased as the lattice rod diameter increases. Furthermore, the densification appears much earlier, and the enhanced energy absorption δEA of the hybrid LEMT structure with respect to the summation of the empty tube and lattice structures is increased as the lattice rod diameter gets larger. This illustrates that the interaction between lattice and tube plays a crucial role in the crashworthiness of the hybrid LEMT structures, and its contribution is enlarged as the lattice rod diameter increases.

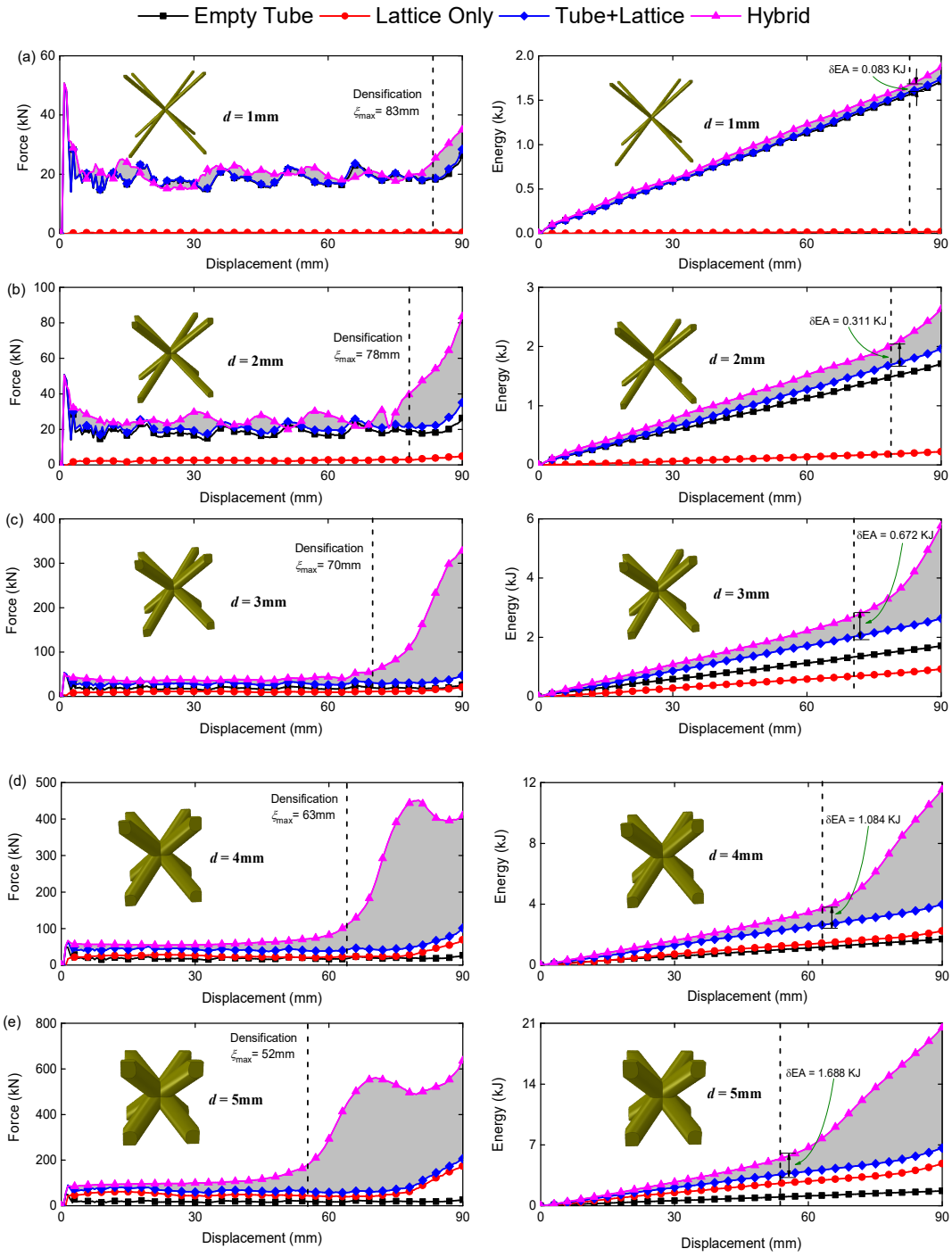

Fig. 11. Force-displacement and energy-displacement curves for hybrid LEMT structures with different lattice rod diameters: (a) d = 1 mm; (b) d = 2 mm; (c) d = 3 mm; (d) d = 4 mm; (e) d = 5 mm. The grey shaded area denotes the enhanced force and EA of hybrid LEMT structures with respect to the summation of their individual constituents. As the lattice rod diameter enlarges, the maximum crushing distance ξ_{max} is reduced, while the enhancement of energy absorption δEA is increased.

To further explain the influence of tube and lattice dimensions on the energy absorption of

hybrid LEMT structures, the influence of wall thickness t and lattice rod diameter d on the SEA is shown in Fig. 12. The energy absorption capacities of empty tubes are almost equal to that of the hybrid LEMT structures when the lattice rod diameter is equal to 1mm. This illustrates that the addition of lattice structure with small rod diameter has little effect on the energy absorption performance of the hybrid LEMT structures. For lattice rod diameter d = 2mm and 3mm, the SEA of hybrid LEMT structures is larger than that of empty tubes, suggesting that the crushing behavior is dominated by the lattice structures. However, the SEA of hybrid LEMT structures becomes smaller than that of empty tubes as lattice rod diameter is larger than 4mm under t = 1.5mm and 2.0mm due to the reduced maximum crushing distance ξ_{max}. Particularly, the SEA of hybrid LEMT structures first increase and then decrease as the lattice rod diameter gets larger, indicating that an optimal SEA can be achieved, which is at d = 3mm. Furthermore, the wall thickness t also plays a significant role on the energy absorption capabilities where the SEA of hybrid LEMT structures increases as the wall thickness gets larger.

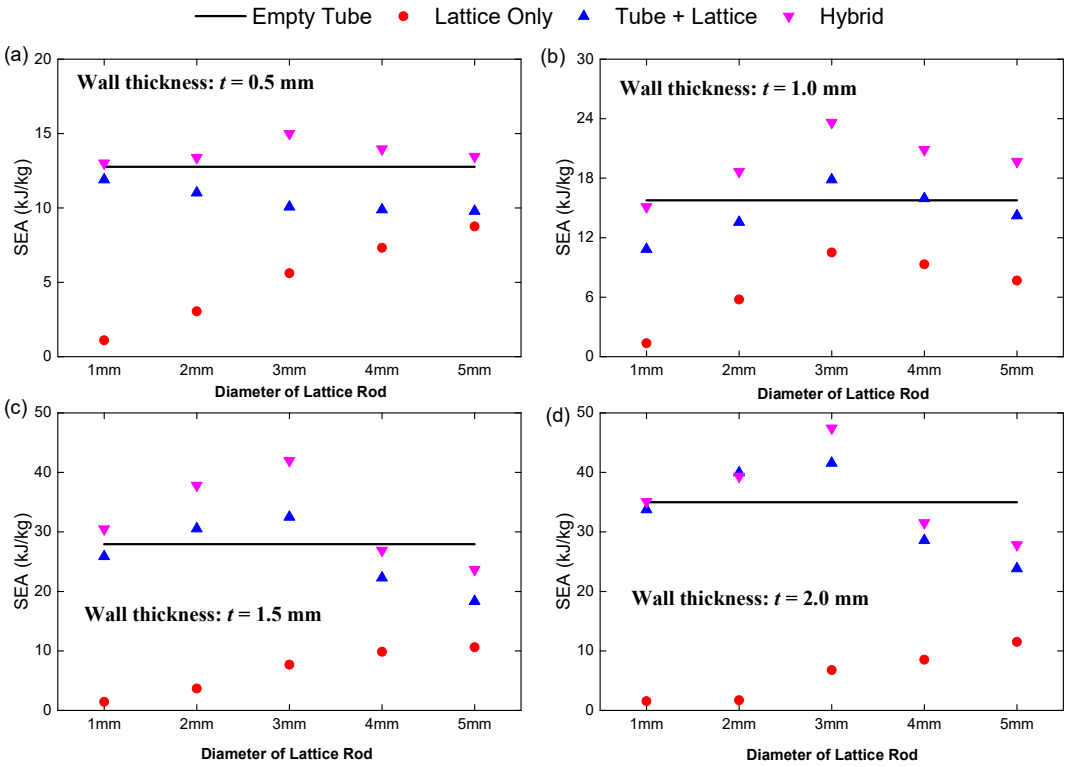

Fig. 12. SEA versus lattice rod diameter for different wall thicknesses of hybrid LEMT structure: (a) t = 0.5 mm; (b) t = 1 mm; (c) t = 1.5 mm; (d) t = 2.0 mm. It is suggested that an optimal SEA can be obtained when the lattice rod diameter equals 3mm.

The CFE of hybrid LEMT structure with different wall thicknesses t and lattice rod diameters

d is depicted in Fig. 13. The CFE is enlarged as the lattice rod diameter d is increased, but with diminishing returns. The enhancement of CFE for the hybrid LEMT structure against the sum of individual parts is significant for d = 3 ~ 5 mm under the wall thickness of $t \leq$ 1.5 mm. This enhancement is less significant under t = 2.0 mm, which suggests that geometrical parameters should be properly designed to obtain the best crashworthiness performance of hybrid LEMT structures.

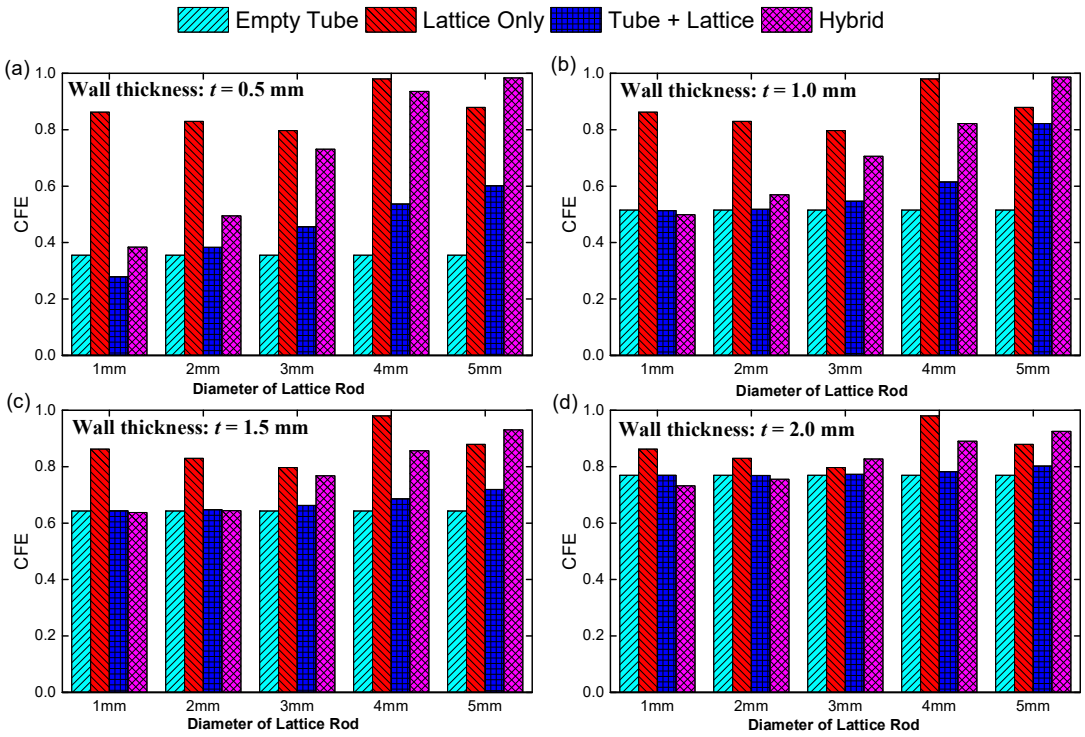

Fig. 13. CFE versus lattice rod diameter of hybrid LEMT structures for different wall thicknesses of tube: (a) t = 0.5 mm; (b) t = 1 mm; (c) t = 1.5 mm; (d) t = 2.0 mm. As the lattice rod diameter is increased, CFE is enlarged but with diminishing returns.

The deformation modes of hybrid LEMT structures under different geometrical parameters for compressive strain of ε = 0.3 are summarized in Table 2, where progressive deformation pattern is observed for all geometrical parameters. For wall thickness t of 0.5 mm and 1 mm, the folding deformation first appears in the middle of the hybrid LEMT structure across different lattice rod diameters. However, for the case with lattice rod diameter d = 1mm, deformation occurs simultaneously in the top and bottom layers. For thicker walls of 1.5 mm and 2.0 mm, the folding deformation first occurs at the top of the hybrid LEMT structures.

Table 2 Deformation modes of hybrid LEMT structure with different geometries for ε = 0.3. Progressive deformation pattern is observed for all geometrical parameters.

Parameters	t = 0.5 mm	t = 1.0 mm	t = 1.5 mm	t = 2.0 mm
d = 1 mm	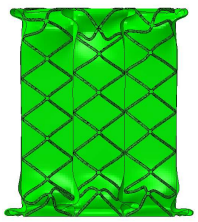	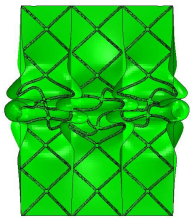		
d = 2 mm	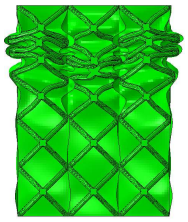	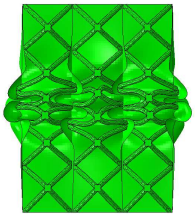		
d = 3 mm	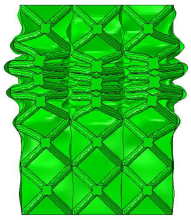	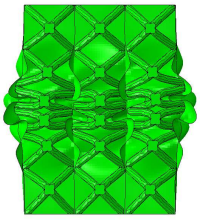		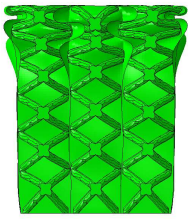
d = 4 mm	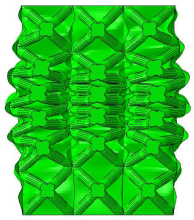	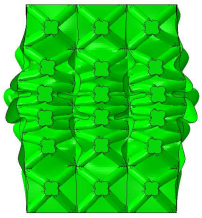	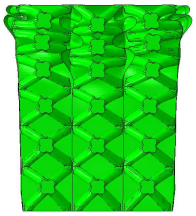	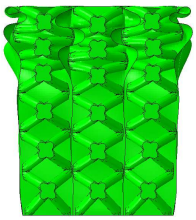

5.3. Height-to-width ratio

The influence of height-to-width ratio on the crushing performances of the hybrid LEMT structure is investigated. Here, the variation in height-to-width ratio is achieved by changing the height of the tube structure to accommodate different numbers of BCC unit (the dimension for each lattice unit is the same), and three hybrid LEMT structures with 6, 12, and 18 BCC units along the longitudinal direction (i.e., three height-to-width ratios of 6:3, 12:3, and 18:3) are considered. The tube wall thickness and lattice rod diameter are fixed at 1 mm and 3 mm, respectively. The force-displacement and EA-displacement performances of these three cases are compared in Fig. 14. One can find that the total EA and maximum crushing distance ξ_{max} of hybrid LEMT structure are both enhanced as the height-to-width ratio is increased due to the increment in

number of BCC units. The enhancement of energy absorption δEA with respect to the sum of individual parts first increases and then decreases as the height-to-width ratio gets larger. This is due to the appearance of global buckling phenomenon at large height-to-width ratios, which are clearly displayed in Table 3. As observed from Table 3, progressive deformation occurs at small height-to-width ratios, while a slightly global instability happens when the height-to-width ratio increases to 12:3, which evolves into global buckling as the height-to-width ratio reaches 18:3.

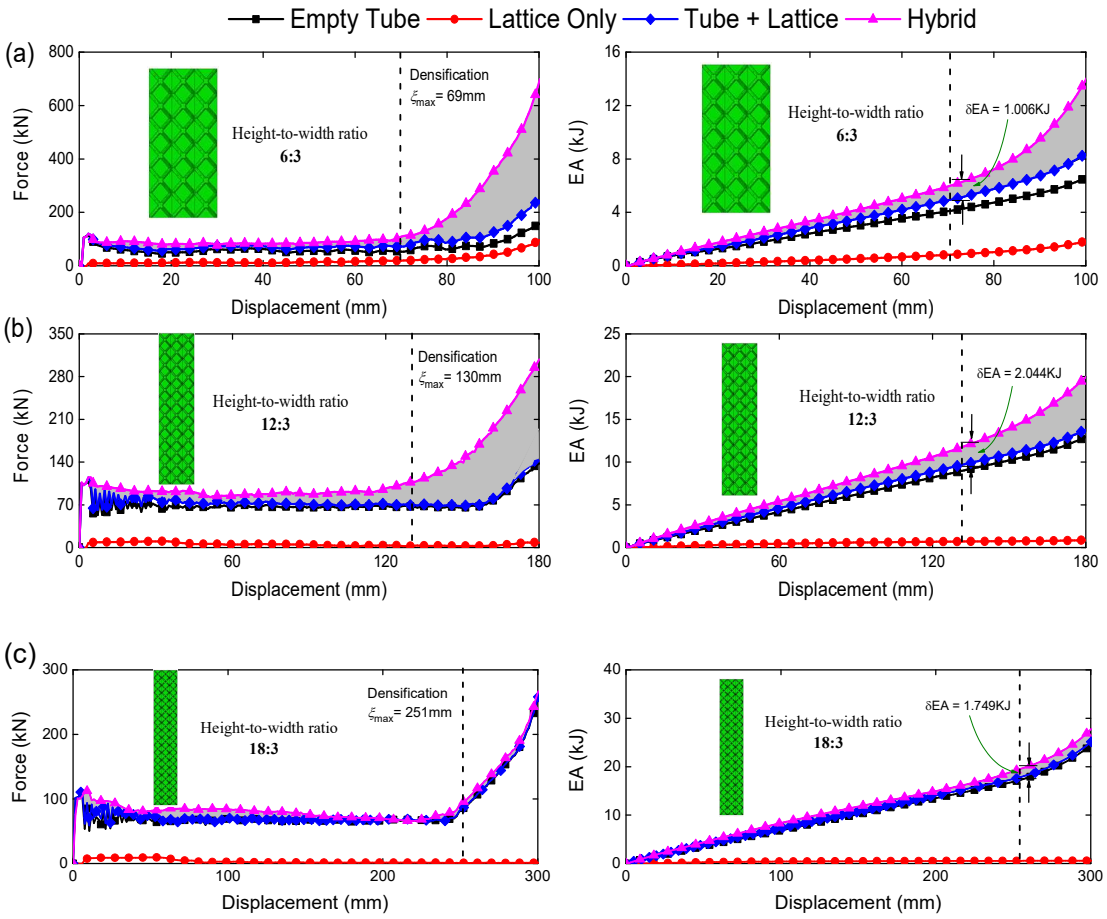

Fig. 14. Force-displacement and EA-displacement curves for hybrid LEMT structures with different height-to-width ratios: (a) 6:3; (b) 12:3; (c) 18:3. The grey shaded area denotes the enhanced force and EA of hybrid LEMT structures with respect to the summation of their individual constituents. As the height-to-width ratio increases, the maximum crushing distance ξ_{max} is enhanced, while the enhancement of energy absorption δEA first increases and then decreases due to the global buckling.

Table 3. Deformation process of hybrid LEMT structures with different height-to-width ratios. Progressive deformation occurs at height-to-width ratio of 6:3, while a slightly global instability happens when the height-to-width ratio increases to 12:3, which then evolves into global buckling as the height-to-width ratio reaches 18:3.

Ratio	$\varepsilon = 0$	$\varepsilon = 0.3$	$\varepsilon = 0.5$	$\varepsilon = 0.7$

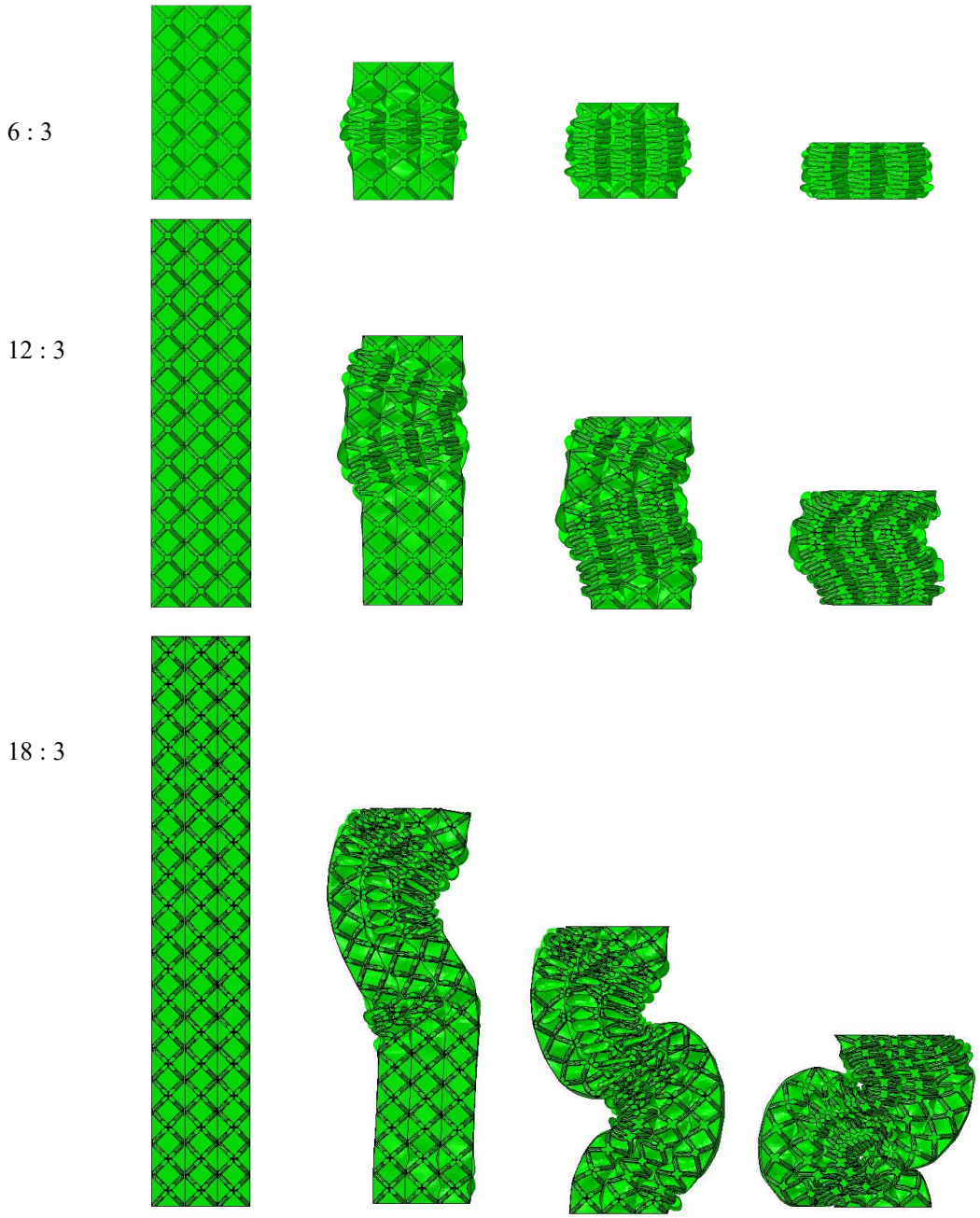

The influence of height-to-width ratio on the SEA and CFE of hybrid LEMT structures is shown in Fig. 15. It is evident that the CFE of the hybrid LEMT structure is always larger than that of the empty tube, illustrating improvements to CFE of multi-cell tubes through the embedded lattice structures. However, the SEA of hybrid LEMT structures is smaller than that of empty tube under the height-to-width ratios of 12:3 and 18:3. This indicates that increasing the number of BCC units along the height direction does not always enhance the SEA performance of hybrid

LEMT structures, and the height-to-width ratio should be bounded to avoid deformation through global buckling.

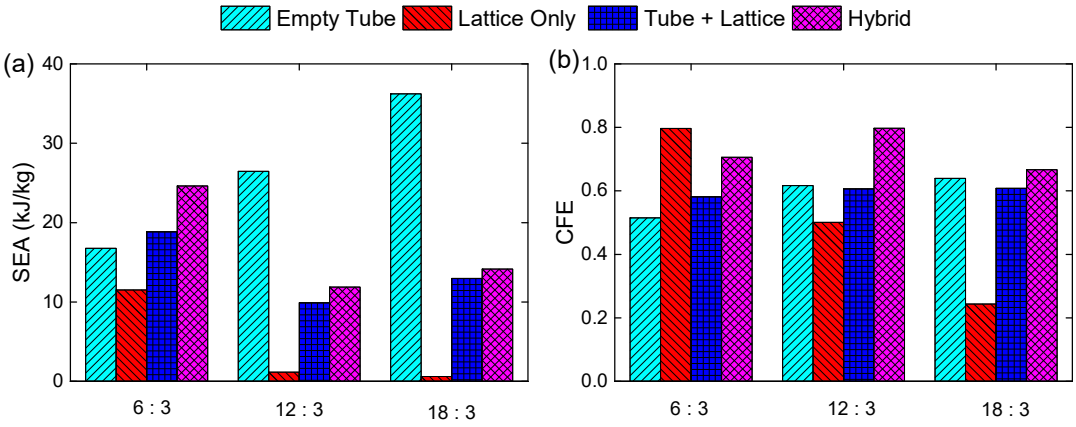

Fig. 15. (a) SEA and (b) CFE of hybrid LEMT structures with different height-to-width ratios. The SEA of hybrid LEMT structures becomes smaller under the height-to-width ratios of 12:3 and 18:3 due to the global buckling.

5.4. Graded lattice vs. uniform lattice

The crushing performances of multi-cell tubes enhanced with graded lattice structure (GLS) and uniform lattice structure (ULS) are compared for their crashworthiness behaviors. The GLS is achieved by varying the lattice rod diameter in each layer following Eq. (1), and the taper angle is set as α = 0.6. Two graded configurations, one with weak top and the other with strong top are taken into account, and the wall thickness t is fixed as 1 mm. By comparing the force-displacement and EA-displacement curves in Fig. 16, the total energy absorption of the hybrid LEMT structure with graded configurations (GLS) is slightly lower than that of ULS due to the smaller total mass of the former. However, the maximum crushing distance ξ_{max} of the two GLS configurations is much larger than that of the ULS, leading to the enhancement of energy absorption δEA of hybrid LEMT structure to the summation of empty tube and lattice structures is slightly enhanced for the GLS.

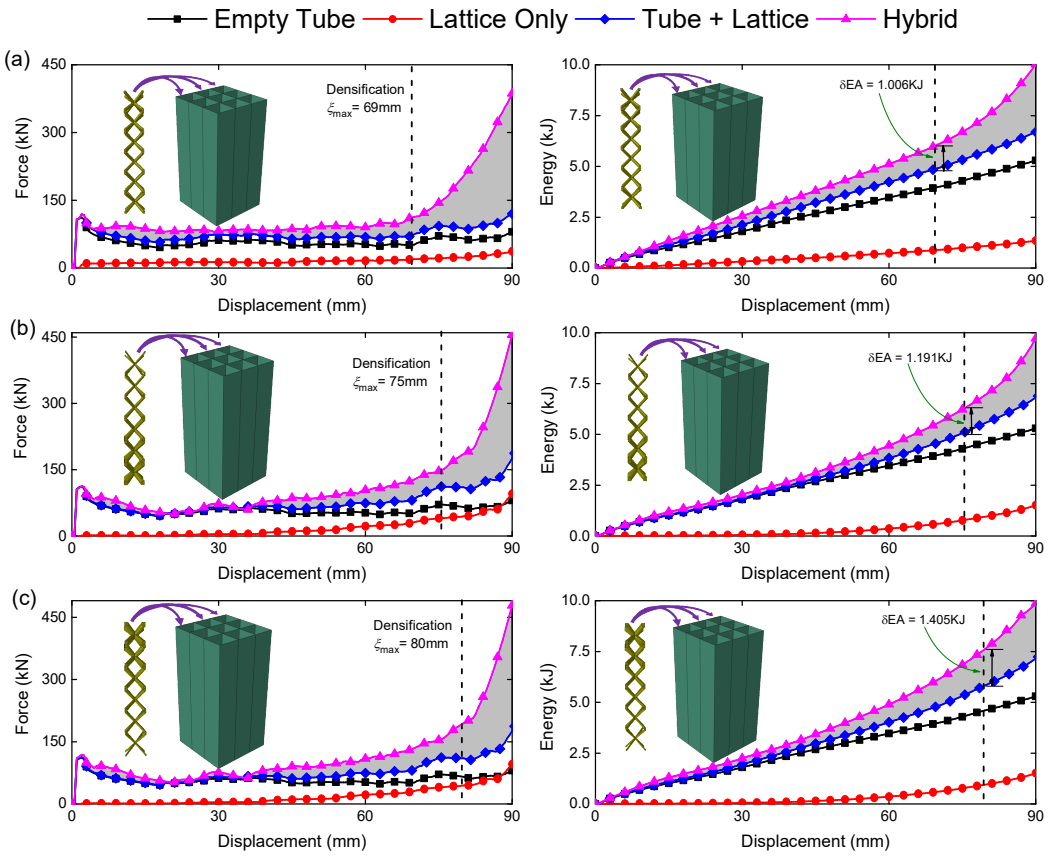

Fig. 16. Force-displacement and EA-displacement curves for hybrid LEMT structures with different lattice configurations: (a) ULS; (b) GLS (weak top); (c) GLS (strong top). The grey shaded area denotes the enhanced force and EA of hybrid LEMT structures with respect to the summation of their individual constituents. The graded lattice design can enlarge both the maximum crushing distance ξ_{max} and the enhancement of energy absorption δEA.

The influence of lattice configuration on SEA and CFE of hybrid LEMT structures is presented in Fig. 17. The SEA of multi-cell tube structure filled with graded lattice is larger than that of its uniform lattice counterpart, and having a strong top at the impact end can provide much better SEA performances. From Fig. 17(b), the graded lattice design slightly decreases the CFE of the hybrid LEMT structures, and the GLS design with the strong top in impact end exhibits larger CFE as compared to the weak top in impact end.

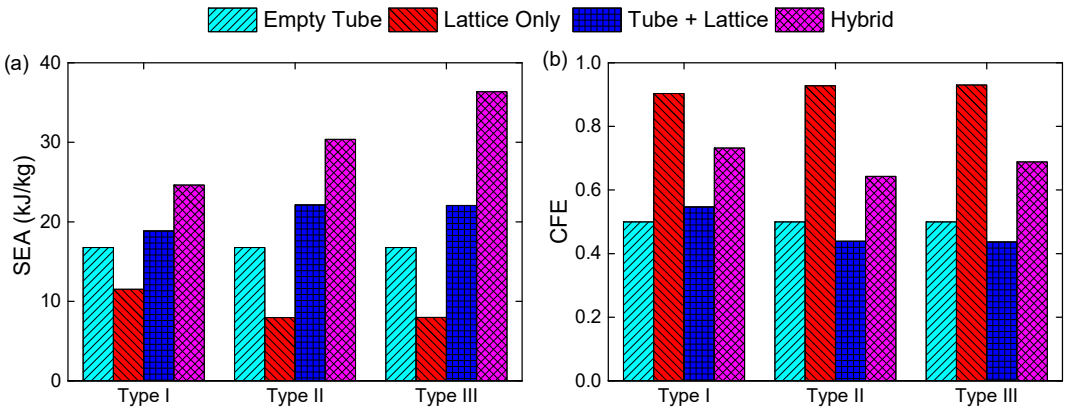

Fig. 17. (a) SEA and (b) CFE of hybrid LEMT structures with different lattice configurations, in which Types I, II, and III represent ULS, GLS (weak top), and GLS (strong top), respectively. The graded lattice configurations perform better than the uniform lattice in terms of SEA, and the strong top in the impact end can provide much larger SEA. However, graded lattice designs slightly decrease the CFE of the hybrid LEMT structures.

The crushing deformation patterns can be clearly observed in Table 4 where the GLS behaves differently from ULS configuration. In the case of the GLS, it can be observed that the structure begins its deformation at the weak end (thinnest lattice rod diameter) and progresses towards the strong end (thickest lattice rod diameter). This crushing behavior seems to be much more predictable for GLS designs.

Table 4. Deformation process of hybrid LEMT structures with different lattice configurations. Structure begins its deformation at the weak end (thinnest lattice rod diameter) and progresses towards the strong end (thickest lattice rod diameter).

Type	$\varepsilon = 0$	$\varepsilon = 0.3$	$\varepsilon = 0.5$	$\varepsilon = 0.7$
ULS	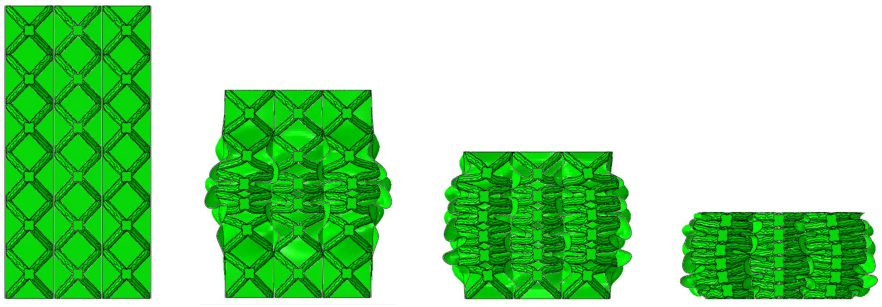			

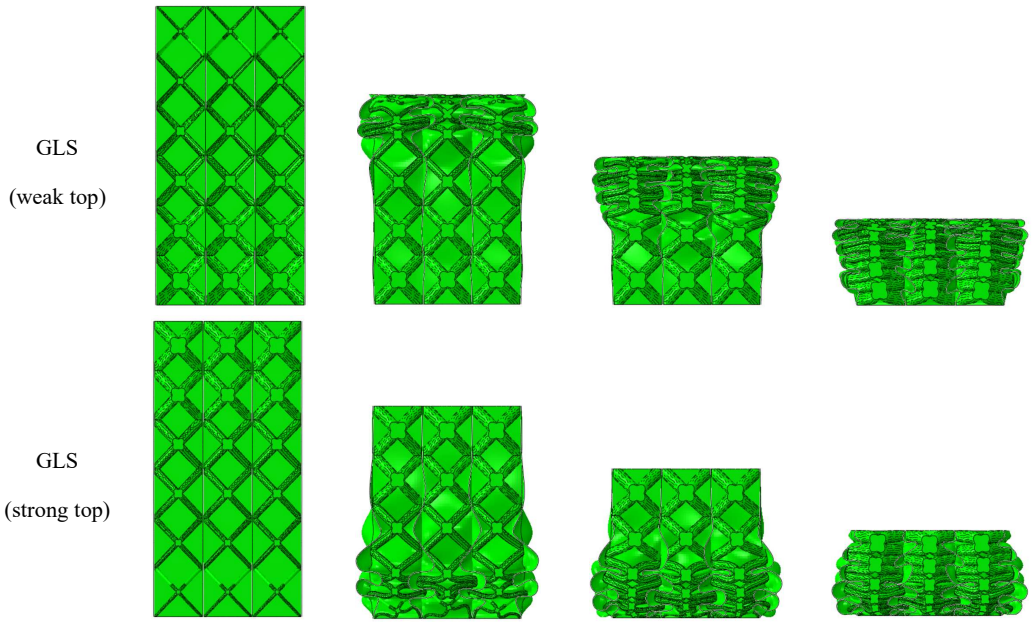

5.5. Taper angle of GLS

To further understand the influence of graded lattice structures on improving the crushing performance of hybrid GLS structures, the influence of taper angle is investigated. The GLS with strong top is illustrated and the wall thickness is specified as t = 1 mm. As shown in Fig. 18, it is evident that the taper angle plays a dominant role in the force-displacement and EA-displacement curves of hybrid LEMT structures. As the taper angle of GLS decreases, the plateau force in the force-displacement curve enlarges, leading to a large increment in the energy absorption for the hybrid LEMT structures. By reducing the taper angle, the densification appears much earlier, i.e., the maximum crushing distance ξ_{max} decreases due to the enhancement of total mass of the lattice structures. In contrast, the enhancement of energy absorption δEA of hybrid LEMT structure to the summation of empty tube and lattice structures is enlarged by decreasing the taper angle.

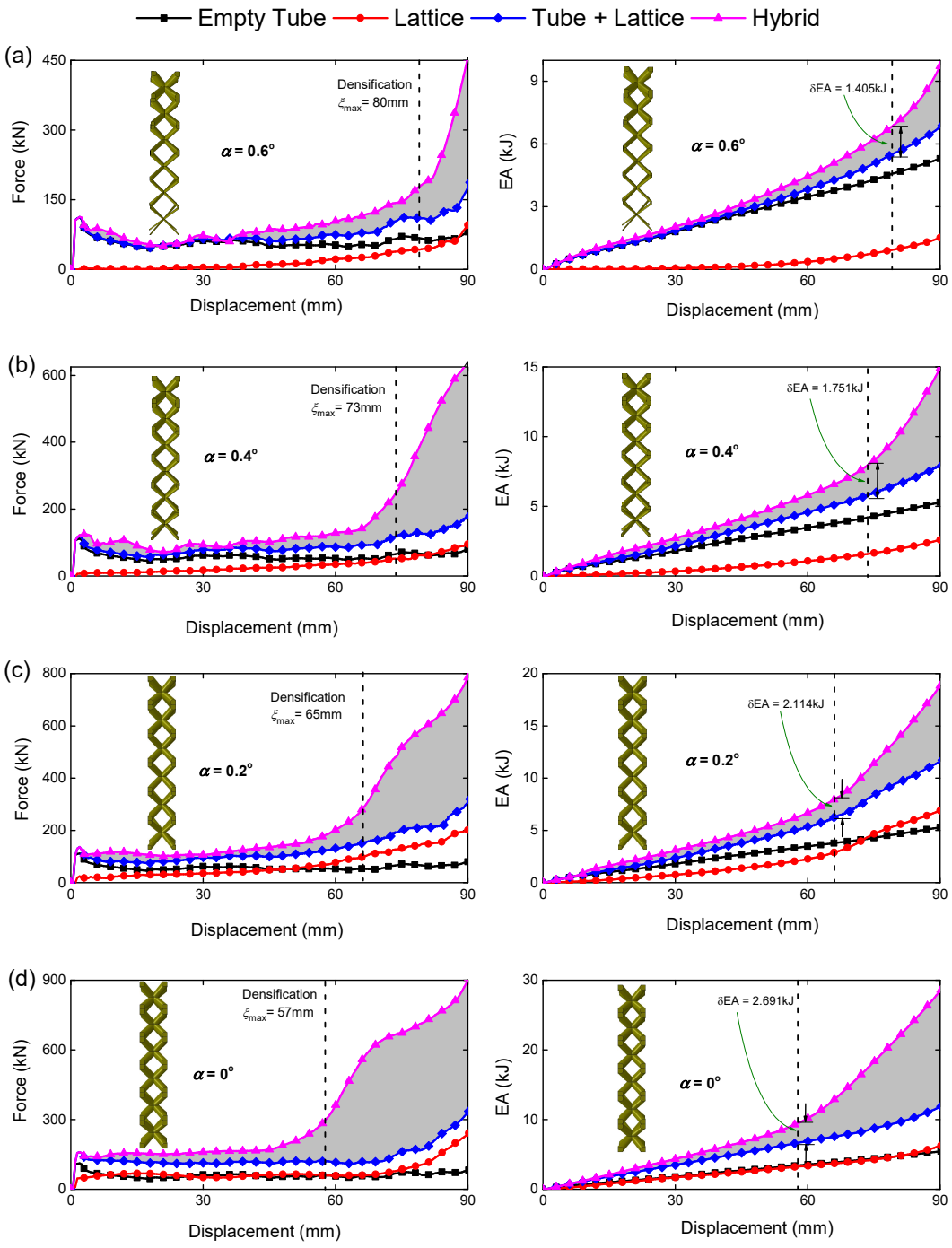

Fig. 18. Force-displacement and EA-displacement curves for GLS structures with varying taper angles: (a) 0.6°; (b) 0.4°; (c) 0.2°; (d) 0°. The grey shaded area denotes the enhanced force and EA of hybrid LEMT structures with respect to the summation of their individual constituents. The maximum crushing distance ξ_{max} reduces, while the enhancement of energy absorption δEA increases by decreasing the taper angle.

The SEA and CFE of the empty tube, sum of empty tube and lattice, and hybrid structures with seven different taper angles, i.e., 0.6°, 0.5°, 0.4°, 0.3°, 0.2°, 0.1° and 0° are investigated in

Fig. 19. It is observed that the SEA of hybrid GLS structures decreases as the taper angle is reduced, while the CFE exhibits an opposite trend. This illustrates that increased taper angles can enhance the energy absorption performance of hybrid GLS structures.

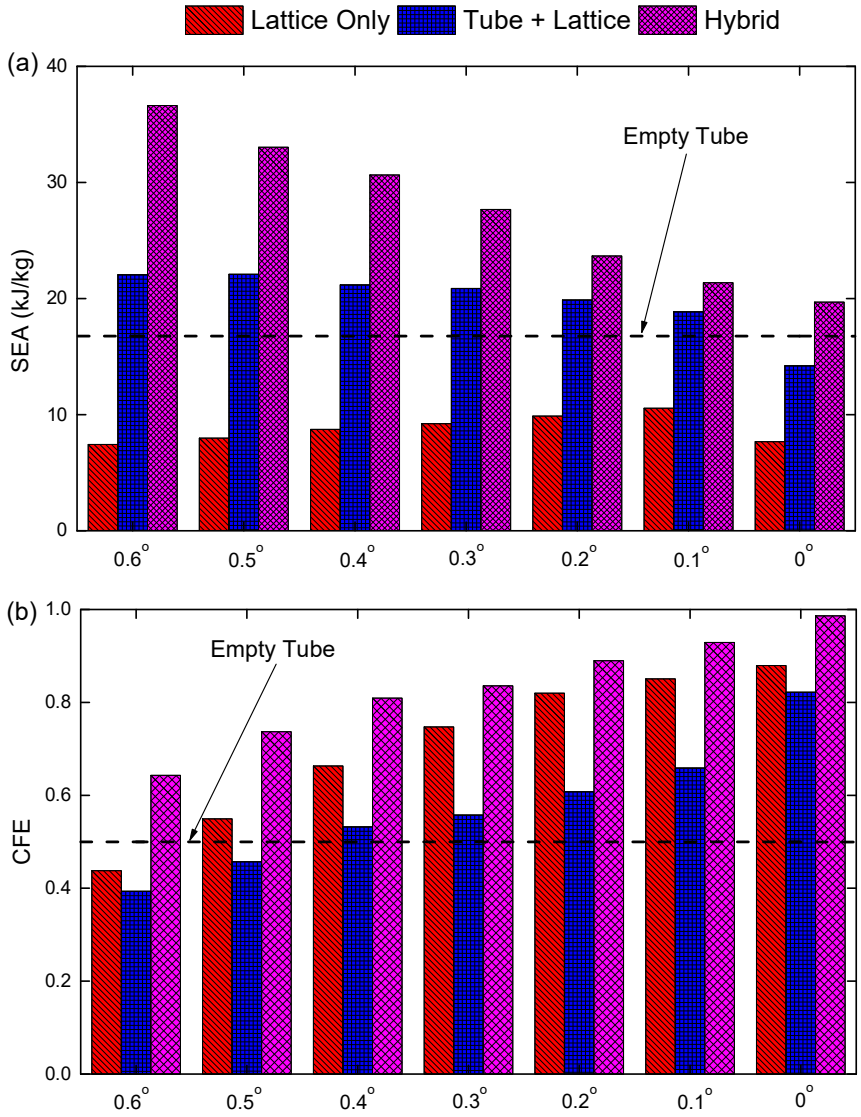

Fig. 19. (a) SEA and (b) CFE versus taper angle of hybrid GLS structure. As illustrated, the taper angle can enhance the SEA and reduces the CFE of hybrid GLS structures.

6. Conclusions

In this work, the crashworthiness performance of multi-cell thin-walled tube enhanced by lattice structures is systematically investigated through a numerical approach. Both uniform and graded lattice structures are filled into the multi-cell thin-walled tube to enhance its energy absorption behaviours. Firstly, the numerical model is validated by comparing with previous

experiments. Subsequently, a comprehensive analysis is conducted to explore the influence of the cell number of tube, the dimension of tube and lattice, the height-to-width ratio of the enhanced tube system, and the configuration of graded lattices on the crushing response of lattice filled multi-cell tube system.

It is demonstrated that the hybrid LEMT structures can absorb more energy than the summation of their individual components due to the interaction between the tube and lattice structures. The enhancements in SEA and CFE are as high as 78.6% and 25.9%, respectively. The energy absorption of the hybrid LEMT structure becomes larger as the number of unit cells and wall thickness of the tube are increased. The addition of lattice structure does not significantly affect SEA of the hybrid LEMT structures when the lattice rod diameter is smaller than 1 mm. However, an optimal SEA of hybrid LEMT structures can be identified when the lattice rod diameter is 3mm.

In addition, increasing the number of BCC units does not always enhance the SEA performance of hybrid LEMT structures. Mild levels of global buckling appear as the height-to-width ratio increases to 12:3, which evolves into full global buckling as the height-to-width ratio increases further. The graded lattice configuration enhances the SEA of hybrid LEMT structures as compared to its uniform counterpart, and having a strong top at the impact end can provide the largest SEA. The crushing behavior is also much more predictable for the graded lattice fillings. The SEA of hybrid LEMT structures enhances as the taper angle is enlarged.

Acknowledgments

The authors would like to thank the Singapore Centre for 3D Printing, which is supported by the National Research Foundation, Prime Minister's Office, Singapore under its Medium-Sized Centre funding scheme, as well as the internal funding by Nanyang Technological University 04INS000329C160 and 04INS000453C160.

References

[1] Ming S, Zhou C, Li T, Song Z, Wang B. Energy absorption of thin-walled square tubes designed by kirigami approach. International Journal of Mechanical Sciences 2019;157-158:150-64.

[2] Hussein RD, Ruan D, Lu G, Thomson R. An energy dissipating mechanism for crushing square aluminium/CFRP tubes. Composite Structures 2018;183:643-53.

[3] Lu R, Liu X, Chen S, Xu Z, Hu X, Liu L. Theoretical investigation on the crushing performances of

tailor rolled tubes with continuously varying thickness and material properties. International Journal of Mechanical Sciences 2019;151:106-17.
[4] Ren Y, Jiang H, Liu Z. Evaluation of double- and triple-coupled triggering mechanisms to improve crashworthiness of composite tubes. International Journal of Mechanical Sciences 2019;157-158:1-12.
[5] Alexander JM. An Approximate Analysis of the Collapse of Thin Cylindrical Shells under Axial Loading. The Quarterly Journal of Mechanics and Applied Mathematics 1960;13:10-5.
[6] Xie S, Chen P, Wang N, Wang J, Du X. Crashworthiness study of circular tubes subjected to radial extrusion under quasi-static loading. International Journal of Mechanical Sciences 2021;192:106128.
[7] Ataabadi PB, Karagiozova D, Alves M. Crushing and energy absorption mechanisms of carbon fiber-epoxy tubes under axial impact. International Journal of Impact Engineering 2019;131:174-89.
[8] Yang H, Lei H, Lu G, Zhang Z, Li X, Liu Y. Energy absorption and failure pattern of hybrid composite tubes under quasi-static axial compression. Composites Part B: Engineering 2020;198:108217.
[9] Pirmohammad S, Esmaeili-Marzdashti S. Multi-objective crashworthiness optimization of square and octagonal bitubal structures including different hole shapes. Thin-Walled Structures 2019;139:126-38.
[10] Fan Z, Lu G, Yu T, Liu K. Axial crushing of triangular tubes. International Journal of Applied Mechanics 2013;5:1350008.
[11] Li Z, Yao S, Ma W, Xu P, Che Q. Energy-absorption characteristics of a circumferentially corrugated square tube with a cosine profile. Thin-Walled Structures 2019;135:385-99.
[12] Deng X, Liu W. Multi-objective optimization of thin-walled sandwich tubes with lateral corrugated tubes in the middle for energy absorption. Thin-Walled Structures 2019;137:303-17.
[13] Ge CQ, Gao Q, Wang LM. Theoretical and numerical analysis of crashworthiness of elliptical thin-walled tube. International Journal of Mechanical Sciences 2018;148:467-74.
[14] Alavi Nia A, Haddad Hamedani J. Comparative analysis of energy absorption and deformations of thin walled tubes with various section geometries. Thin-Walled Structures 2010;48:946-54.
[15] Zhao X, Zhu G, Zhou C, Yu Q. Crashworthiness analysis and design of composite tapered tubes under multiple load cases. Composite Structures 2019;222:110920.
[16] Alkhatib SE, Tarlochan F, Hashem A, Sassi S. Collapse behavior of thin-walled corrugated tapered tubes under oblique impact. Thin-Walled Structures 2018;122:510-28.
[17] San Ha N, Lu G, Xiang X. High energy absorption efficiency of thin-walled conical corrugation tubes mimicking coconut tree configuration. International Journal of Mechanical Sciences 2018;148:409-21.
[18] Ha NS, Lu G. Thin-walled corrugated structures: A review of crashworthiness designs and energy absorption characteristics. Thin-Walled Structures 2020;157:106995.
[19] Ye H, Ma J, Zhou X, Wang H, You Z. Energy absorption behaviors of pre-folded composite tubes with the full-diamond origami patterns. Composite Structures 2019;221:110904.
[20] Kim H-S. New extruded multi-cell aluminum profile for maximum crash energy absorption and weight efficiency. Thin-Walled Structures 2002;40:311-27.
[21] Zhang X, Zhang H, Yang C, Leng K. Static and dynamic axial crushing of self-locking multi-cell tubes. International Journal of Impact Engineering 2019;127:17-30.
[22] Zhang X, Leng K, Zhang H. Axial crushing of embedded multi-cell tubes. International Journal of Mechanical Sciences 2017;131-132:459-70.
[23] Zhang X, Zhang H. Some problems on the axial crushing of multi-cells. International Journal of

Mechanical Sciences 2015;103:30-9.
[24] Fu J, Liu Q, Liufu K, Deng Y, Fang J, Li Q. Design of bionic-bamboo thin-walled structures for energy absorption. Thin-Walled Structures 2019;135:400-13.
[25] Zhang Y, Wang J, Wang C, Zeng Y, Chen T. Crashworthiness of bionic fractal hierarchical structures. Materials & Design 2018;158:147-59.
[26] Hu D, Wang Y, Song B, Dang L, Zhang Z. Energy-absorption characteristics of a bionic honeycomb tubular nested structure inspired by bamboo under axial crushing. Composites Part B: Engineering 2019;162:21-32.
[27] Wang J, Zhang Y, He N, Wang CH. Crashworthiness behavior of Koch fractal structures. Materials & Design 2018;144:229-44.
[28] Wang Z, Zhang J, Li Z, Shi C. On the crashworthiness of bio-inspired hexagonal prismatic tubes under axial compression. International Journal of Mechanical Sciences 2020;186:105893.
[29] Chen BC, Zou M, Liu GM, Song JF, Wang HX. Experimental study on energy absorption of bionic tubes inspired by bamboo structures under axial crushing. International Journal of Impact Engineering 2018;115:48-57.
[30] Li Z, Ma W, Xu P, Yao S. Crashworthiness of multi-cell circumferentially corrugated square tubes with cosine and triangular configurations. International Journal of Mechanical Sciences 2020;165:105205.
[31] Huang Z, Zhang X, Yang C. Static and dynamic axial crushing of Al/CRFP hybrid tubes with single-cell and multi-cell sections. Composite Structures 2019;226:111023.
[32] Hu D, Wang Y, Song B, Wang Y. Energy absorption characteristics of a foam-filled tri-tube under axial quasi-static loading: experiment and numerical simulation. International Journal of Crashworthiness 2017;23:417-32.
[33] Fang J, Gao Y, Sun G, Qiu N, Li Q. On design of multi-cell tubes under axial and oblique impact loads. Thin-Walled Structures 2015;95:115-26.
[34] Yang X, Ma J, Sun Y, Yang J. An internally nested circular-elliptical tube system for energy absorption. Thin-Walled Structures 2019;139:281-93.
[35] Wang Z, Li Z, Zhang X. Bending resistance of thin-walled multi-cell square tubes. Thin-Walled Structures 2016;107:287-99.
[36] Wang Z, Zhang X, Li Z. Bending collapse of multi-cell tubes. International Journal of Mechanical Sciences 2017;134:445-59.
[37] Zhang X, Zhang H, Leng K. Experimental and numerical investigation on bending collapse of embedded multi-cell tubes. Thin-Walled Structures 2018;127:728-40.
[38] Santosa SP, Wierzbicki T, Hanssen AG, Langseth M. Experimental and numerical studies of foam-filled sections. International Journal of Impact Engineering 2000;24:509-34.
[39] Duarte I, Krstulović-Opara L, Dias-de-Oliveira J, Vesenjak M. Axial crush performance of polymer-aluminium alloy hybrid foam filled tubes. Thin-Walled Structures 2019;138:124-36.
[40] Yalçın MM, Genel K. On the axial deformation characteristic of PVC foam-filled circular aluminium tube: Effect of radially-graded foam filling. Thin-Walled Structures 2019;144:106335.
[41] Li S, Guo X, Liao J, Li Q, Sun G. Crushing analysis and design optimization for foam-filled aluminum/CFRP hybrid tube against transverse impact. Composites Part B: Engineering 2020;196:108029.
[42] Yi Z, Si-yuan H, Jia-gui L, Wei Z, Xiao-lu G, Jin Y. Density gradient tailoring of aluminum foam-filled tube. Composite Structures 2019;220:451-9.

[43] Wang L, Zhang B, Zhang J, Jiang Y, Wang W, Wu G. Deformation and energy absorption properties of cenosphere-aluminum syntactic foam-filled tubes under axial compression. Thin-Walled Structures 2021;160:107364.
[44] Zhang B, Wang L, Zhang J, Jiang Y, Wang W, Wu G. Deformation and energy absorption properties of cenosphere/aluminum syntactic foam-filled circular tubes under lateral quasi-static compression. International Journal of Mechanical Sciences 2021;192:106126.
[45] Yang H, Lei H, Lu G. Crashworthiness of circular fiber reinforced plastic tubes filled with composite skeletons/aluminum foam under drop-weight impact loading. Thin-Walled Structures 2021;160:107380.
[46] Liu Z, Huang Z, Qin Q. Experimental and theoretical investigations on lateral crushing of aluminum foam-filled circular tubes. Composite Structures 2017;175:19-27.
[47] Liu Q, Xu X, Ma J, Wang J, Shi Y, Hui D. Lateral crushing and bending responses of CFRP square tube filled with aluminum honeycomb. Composites Part B: Engineering 2017;118:104-15.
[48] Wang H, Su M, Hao H. The quasi-static axial compressive properties and energy absorption behavior of ex-situ ordered aluminum cellular structure filled tubes. Composite Structures 2020;239:112039.
[49] Dong M, Elchalakani M, Karrech A, Hassanein MF, Xie T, Yang B. Behaviour and design of rubberised concrete filled steel tubes under combined loading conditions. Thin-Walled Structures 2019;139:24-38.
[50] Liang W, Dong J, Wang Q. Mechanical behaviour of concrete-filled double-skin steel tube (CFDST) with stiffeners under axial and eccentric loading. Thin-Walled Structures 2019;138:215-30.
[51] Zheng Y, Tao Z. Compressive strength and stiffness of concrete-filled double-tube columns. Thin-Walled Structures 2019;134:174-88.
[52] Drücker S, Schulze M, Ipsen H, Bandegani L, Hoch H, Kluge M, et al. Experimental and numerical mechanical characterization of additively manufactured Ti6Al4V lattice structures considering progressive damage. International Journal of Mechanical Sciences 2021;189:105986.
[53] Jin N, Yan Z, Wang Y, Cheng H, Zhang H. Effects of heat treatment on microstructure and mechanical properties of selective laser melted Ti-6Al-4V lattice materials. International Journal of Mechanical Sciences 2021;190:106042.
[54] Sun ZP, Guo YB, Shim VPW. Characterisation and modeling of additively-manufactured polymeric hybrid lattice structures for energy absorption. International Journal of Mechanical Sciences 2021;191:106101.
[55] Cetin E, Baykasoğlu C. Energy absorption of thin-walled tubes enhanced by lattice structures. International Journal of Mechanical Sciences 2019;157-158:471-84.
[56] Baykasoğlu A, Baykasoğlu C, Cetin E. Multi-objective crashworthiness optimization of lattice structure filled thin-walled tubes. Thin-Walled Structures 2020;149:106630.
[57] Bai L, Gong C, Chen X, Sun Y, Xin L, Pu H, et al. Mechanical properties and energy absorption capabilities of functionally graded lattice structures: Experiments and simulations. International Journal of Mechanical Sciences 2020;182:105735.
[58] Cetin E, Baykasoğlu C. Crashworthiness of graded lattice structure filled thin-walled tubes under multiple impact loadings. Thin-Walled Structures 2020;154:106849.
[59] Chen W, Wierzbicki T. Relative merits of single-cell, multi-cell and foam-filled thin-walled structures in energy absorption. Thin-Walled Structures 2001;39:287-306.
[60] Googarchin HS, Pasandidehpoor M, Mahmoodi A, Shojaeefard MH. Energy absorption analysis

for tapered multi-cell tubes improved by foams: Theoretical development and numerical simulation. Composite Structures 2019;207:213-22.
[61] Zhang Y, Ge P, Lu M, Lai X. Crashworthiness study for multi-cell composite filling structures. International journal of crashworthiness 2018;23:32-46.
[62] Zhang H, Zhang X. Axial crushing of self-lock multi-cell tubes with foam filler and tube envelope. Thin-Walled Structures 2020;155:106847.
[63] Yin H, Wen G, Liu Z, Qing Q. Crashworthiness optimization design for foam-filled multi-cell thin-walled structures. Thin-Walled Structures 2014;75:8-17.
[64] Sun G, Liu T, Huang X, Zheng G, Li Q. Topological configuration analysis and design for foam filled multi-cell tubes. Engineering Structures 2018;155:235-50.
[65] Zhang X, Cheng G. A comparative study of energy absorption characteristics of foam-filled and multi-cell square columns. International journal of impact engineering 2007;34:1739-52.
[66] Karagiozova D, Nurick GN, Chung Kim Yuen S. Energy absorption of aluminium alloy circular and square tubes under an axial explosive load. Thin-Walled Structures 2005;43:956-82.
[67] Zhang X, Zhang H. Energy absorption of multi-cell stub columns under axial compression. Thin-Walled Structures 2013;68:156-63.
[68] Gibson LJ, Ashby MF. Cellular solids: structure and properties. Cambridge, UK: Cambridge university press; 1997.